Chemical Physics 127 (1988) 399–409
North-Holland, Amsterdam

SCALAR AND VECTOR PROPERTIES OF RO($A\,^2\Sigma^+$) FORMED IN THE VUV PHOTODISSOCIATION OF R_2O_2 (R=H, D)

K.-H. GERICKE, H. GÖLZENLEUCHTER and F.J. COMES
Institut für Physikalische and Theoretische Chemie, Niederurseler Hang, 6000 Frankfurt am Main 50, FRG

Received 21 June 1988

Emission spectroscopy has been applied to study the photofragmentation of hydrogen peroxide and its deuterated analogon. At the photolysis wavelength of 157 nm the parent is excited to a high-lying ^{1}A or ^{1}B state. One of the fragments is formed in the $A\,^2\Sigma^+$ state with a quantum efficiency of 0.07. From the analysis of its fluorescence, $A\,^2\Sigma^+ \rightarrow X\,^2\Pi$, the energy release on the various degrees of freedom is deduced. The products are formed with low vibrational excitation, but the rotational excitation of the fragment is highly inverted and peaks at $N_{OH} \approx 21$ and $N_{OD} \approx 27$ for $v' = 0$. Polarization spectroscopy is used to measure the rotational anisotropy. The alignment parameter is negative for high product rotations and found to be $A_0^{(2)} = -0.25$ indicating a more perpendicular orientation between N and μ, the transition dipole moment of the parent. The major part of fragment rotation is from a torsional dependence of the upper potential surface. Initial parent thermal motion is of minor influence on the rotational excitation of the fragment. Conservation of energy and angular momentum together with the alignment of the fragment leads to the conclusion that the partner product [OR($X\,^2\Pi$)] which is coincidently formed in the same microscopic fragmentation event is also rotationally hot and the two fragments rotate in opposite directions.

1. Introduction

Hydrogen peroxide plays an important role as a main oxidant in atmospheric chemistry. A question of special importance is concerned with its formation in rain drops where HO_x radicals as precursors may lead to the formation of H_2O_2 [1]. Gaseous atmospheric H_2O_2 can be detected by using tunable diode lasers with long-path absorption [2]. Also photodissociation of H_2O_2 in the vacuum UV offers an interesting way for its detection because one of the two OH fragments can be formed as electronically excited species, thus giving rise to the resonance radiation $A\,^2\Sigma^+ \rightarrow X\,^2\Pi$ near 310 nm [3,4].

The fluorescence of the electronically excited product can be analyzed in a state-resolved manner. Furthermore, the use of Doppler and polarization spectroscopy is a powerful method in studying the dynamics of fragmentation processes. Not only the symmetry of the involved electronic states can be determined, but also information on the lifetime of the excited state can be extracted [5,6]. In addition to scalar properties as population of fragments in rotational and vibrational states, the determination of vector correlations between μ, the transition dipole moment of the parent molecule, v the velocity, and J, the rotational moment of the fragment, are an excellent characterization of the photofragmentation process [7].

A substantial progress has been achieved by extending the studies on vector correlations, between product translation and rotation. This $\langle v, J \rangle$ correlation is now related only to the molecular frame and is no longer based on the lab frame. In a four-atomic molecule such as H_2O_2 the correlation between the velocity of the fragments v, and the rotational moment J, is no longer trivial as it is the case of a triatomic molecule where apart from thermal motion the fragment velocity vector lies necessarily in the plane of the molecule with the rotational moment, J, always pointing vertical to it. In H_2O_2, the torsion motion of the OH rotor can be a source of fragment rotation resulting in a parallel orientation between v and J.

The study of fragment vector properties had been concentrated on the first two electronically excited states of the parent H_2O_2, which are the $\tilde{A}\,^1$A and $\tilde{B}\,^1$B states [8–10]. These repulsive states lead to two OH

fragments with low rotational excitation in the electronic ground state $^2\Pi_{3/2,1/2}$. The primary excitation sources were the radiation at 266 nm of the fourth harmonic of a Nd–YAG laser and the two excimer laser wavelengths at 248 and 193 nm. At wavelengths below 172 nm a new dissociation channel is opened from which electronically excited hydroxyl radicals in the $^2\Sigma^+$ state evolve. Therefore, emission spectroscopy can be used to investigate the fragmentation pattern of

$$H_2O_2(\tilde{X}\,^1A) + h\nu \rightarrow OH(X\,^2\Pi) + OH^{\ddagger}(A\,^2\Sigma^+) \quad (1)$$

and its deuterated analogon [11,12].

Earlier measurements showed that 7% of the total absorption is related to reaction (1) and, consequently, the formation of two non-excited radicals is still the major process [3]. The present paper reports on a detailed investigation of the one-photon excitation of R_2O_2 (R=H, D) which leads to $OR(A\,^2\Sigma^+)$ products. Not only the entire internal state distribution was determined, but also the fragment alignment using different polarization excitation and detection schemes.

2. Experimental

The photodissociation studies were carried out as a photoinduced emission experiment. The photolysis source is an F_2 excimer laser operating at 157 nm. At this wavelength the output energy of the laser was 5 mJ at a repetition rate of 10 Hz. The temporal width of a pulse was 10 ns. After 30 min of operation the laser output energy decreased to half of its original value. The laser beam was slightly focused into an aluminium cell by a 300 mm MgF_2 lense. To avoid absorption of the laser radiation by ambient air the light path between the laser and the entrance window of the cell was floated by dry nitrogen gas. A schematic view of the setup is given in fig. 1 which shows the light baffles together with a Woods horn to avoid stray light problems. Vertically to the photolysis beam the $A\,^2\Sigma^+ \rightarrow X\,^2\Pi$ fluorescence light of the excited products is observed. The gas sample is contained in a cell which can be evacuated by a vacuum pump system consisting of a diffusion and a rotary pump.

The fluorescence detecting system consists of a monochromator (0.5 m Minuteman, grating: 3600 g/mm) which carries two exit slit mountings. One of them is used in combination with a photomultiplier detector, while the other one is equipped with an optical multichannel analyzer (OSMA: Physical Instruments Inc.). The quantum efficiency of the photomultiplier between 300 and 400 nm is about 25%. The array of the OSMA system shows a nearly constant quantum efficiency in the near ultraviolet. The OSMA system leads to a small decrease in final resolution of the whole device, compared to the use of the photomultiplier. However, the optical multichannel analyzer monitors a large part of the complete fluorescence spectrum at a single laser shot and the capability of integration over a number of photolysis shots improves the signal-to-noise ratio by more than one order of magnitude.

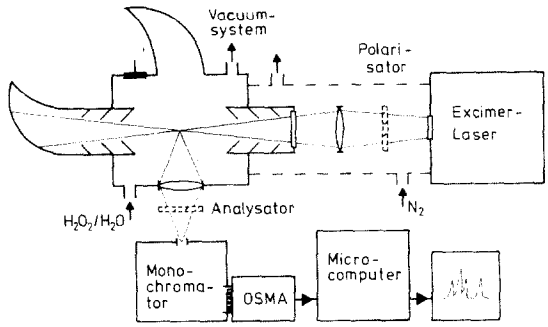

Fig. 1. Schematic diagram of the experimental setup.

With a slit width of 20 μm a resolution of the monochromator of $\lambda/\Delta\lambda = 3\times10^4$ was obtained using the holographic grating of 3600 grooves/mm (Yobin–Ivon). In this high-resolution version the monochromator in combination with the diode array allowed simultaneous detection of a 8.5 nm wide strip of the spectrum. In order to measure simultaneously the complete $A\,^2\Sigma^+ \rightarrow X\,^2\Pi$ spectrum, a grating of lower resolution (600 grooves/mm) was used.

The H_2O_2 probe gas which was passed into the cell was evaporated from a H_2O_2/H_2O solution with a H_2O_2 concentration of more than 98%. This leads to $>75\%$ H_2O_2 purity in the gas phase at room temperature. Control of the concentration of the solution was made by measurement of its refractive index [13]. The probes were obtained by vacuum destillation starting from solutions of 85% purity which were kindly supplied by Degussa. It should be mentioned that the photolysis of the remaining water does not

influence the OH($A\,^2\Sigma^+$) product state distribution, because only at wavelengths below 135 nm water dissociates into electronically excited hydroxyl radicals [14].

The D_2O_2 probes were prepared by proton exchange reactions of highly concentrated H_2O_2/H_2O solution with the deuterium atoms in D_2O. Up concentration of D_2O_2 was again achieved by vacuum destillation. Finally a solution containing D_2O_2 at a purity of 87% was measured. The calculated composition of this solutions is

$$D_2O_2 : HDO_2 : H_2O_2 = 100 : 3 : 0.3.$$

The purity of the D_2O_2 samples used in the photolysis was controlled by search for OH emission in the 157 nm photolysis as well as by studying its photolysis at 266 nm and probing the OH radicals by LIF. These experiments showed that the proton content of the solution is well below 1%.

The peroxides are flown from the reservoir into the cell at a rate of about 1 cm^3 per second to avoid the build up of photolysis products. The reservoir of 250 ml was made of colored glas to prevent the solution from dissociation by daylight. The gas handling system was kept grease free.

When the setup was used to measure the scalar properties, as there are the vibrational and the rotational state distribution, the radiation from the photolysis source as well as the fluorescence light was depolarized by the use of a Hanle scrambler (Halle). In case of polarization experiments the photolysis laser light could be linearly polarized using a MgF_2 Rochon prism and the fluorescence light was detected after passing an other polarizer. All possible combinations of incident (I_i) and fluorescence light (I_f) polarization, vertical or horizontal, result in four cases. However, due to the cylindrical symmetry three of them lead to identical results.

3. Product state distribution

The determination of scalar and vectorial properties of fragmentation events is related to an observation of the nascent fragment distribution. This demands that the spectroscopic data are not spoiled by collisional relaxation. As the mean lifetime of OH radicals in the A($^2\Sigma^+$) state is about 700 ns the total pressure in the observation region has to be rather low [15]. Relaxation processes will have an influence on the lifetime as well as on the fragment state distribution. As the rotation is very sensitive to collisions, observation of fragment lifetimes in isolated rotational states as well as rotational state distributions as a function of total cell pressure is a useful control. Both types of measurement showed that up to 10 mTorr no detectable changes were observed. Even up to 50 mTorr the rotational state distribution remained unchanged. For that reason all experiments were carried out at variable pressures between 1 and 50 mTorr.

Fig. 2 shows the 0–0 band of the OH $A\,^2\Sigma^+ \rightarrow X\,^2\Pi$ transition after excitation of H_2O_2 at 157 nm. The rotational structure of the bands is not always completely resolved and the final rotational state distribution is obtained from simulation calculations.

The $A\,^2\Sigma^+ \rightarrow X\,^2\Pi$ transitions in a vibrational band consist of twelve rotational branches. The spectral positions [3,16] as well as the transition probabilities [17] are all well known so that any of the twelve lines can be used as a source of information on the population of a specific rotational state of quantum number N. To extract that information from the spectrum the shape of the emission lines has to be

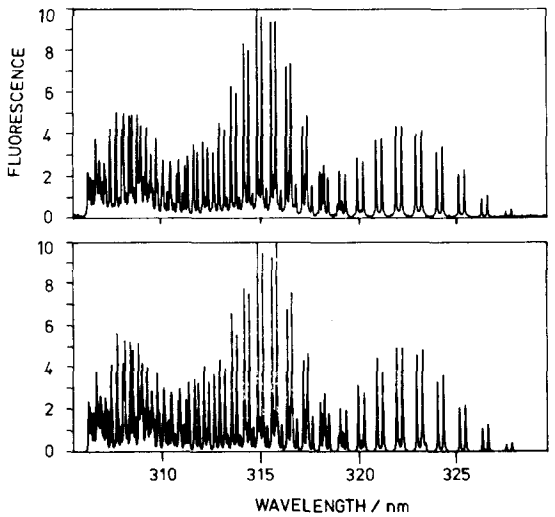

Fig. 2. Fluorescence spectrum of OH $^2\Sigma^+(v'=0) \rightarrow {}^2\Pi(v''=0)$ resulting from the 157 nm photolysis of H_2O_2. Top trace: observed emission band at a total pressure of 10 mTorr; lower trace: computer simulation based upon the OH population numbers and detected line profiles.

well known to successfully run the deconvolution procedure. As there are a number of lines in the spectrum which are completely resolved this condition is easily fulfilled. For better control the experimental line shape was independently determined from a separate measurement using a low-pressure mercury lamp as atomic emission source. From such measurements the relevant line profile is obtained which was the best fit to the experimental line shapes. The line shape is represented by a formula which contains a contribution from both a Gaussian and a Lorentzian line

$$f(\lambda) = \exp[-4 \ln 2\ (\lambda-\lambda_0)^2/b^2] + [1+4(\lambda-\lambda_0)^2/b^2]^{-1},$$

with b, the line width at half-maximum. With the aid of this line shape formula and with relevant population numbers in the rotational states a spectrum is calculated. The intensity differences taken from this spectrum and the measured one are then used to vary the starting conditions systematically using a least-squares fit procedure until the best fit is obtained. In a final proof of the consistence of the calculations, simulations were carried out using different sets of population numbers as starting conditions. In all cases the same final population was obtained. Fig. 2 shows the degree of agreement for the region of the 0–0 transition.

In order to compare the experimental spectrum with calculations it has to be established that the data are not influenced by polarization effects. For that reason care was taken to depolarize the photolysis radiation and the fluorescence radiation as well by suitable optical elements. The remaining alignment in the system due to the use of directed beams will influence the observed population numbers to less than 5%.

There is, however, an additional effect which can spoil the data because fluorescence of the fragments is used as a source of information. Transitions from higher rotational states which appear in the spectrum are effected by predissociation which opens a dark channel ($^2\Sigma^+ \rightarrow {}^4\Sigma^-$) and shortens the lifetime of the excited species. A correction for this effect has to be made for OH, $v'=0$, $N'>23$, and $v'=1$, $N'>14$. Due to the smaller rotational constant of OD this effect starts at considerably higher quantum states ($v'=0$, $N'>37$). The final corrections due to predissociation were made by multiplying the measured intensities by the factor

$$f = 1+\tau_{fl}(N)P_{Pr}(N),$$

with τ_{fl} the radiation lifetime of the fragment in state N and P_{Pr} its predissociation probability [18].

As a result of such calculations we obtain the rotational population in the different vibrational states of OH and OD, which are shown in figs. 3 and 4. The accuracy in the OD data is of course lower compared with the OH data because of the stronger congestion in this spectrum which stems from the smaller rotational constant. These figures indicate that the population is definitely non-Boltzmannian. There exist an obvious preference for higher rotational states.

The vibrational state distribution was obtained from the integrated band intensities. As the contribution from $v'=2$ is only marginal, information is obtained from the 0–0, 1–0 and 1–1 vibrational bands which leads to the data of table 1. This table contains results from H_2O_2 and D_2O_2 as well. The population in the $v'=1$ state is about 10% of the total popula-

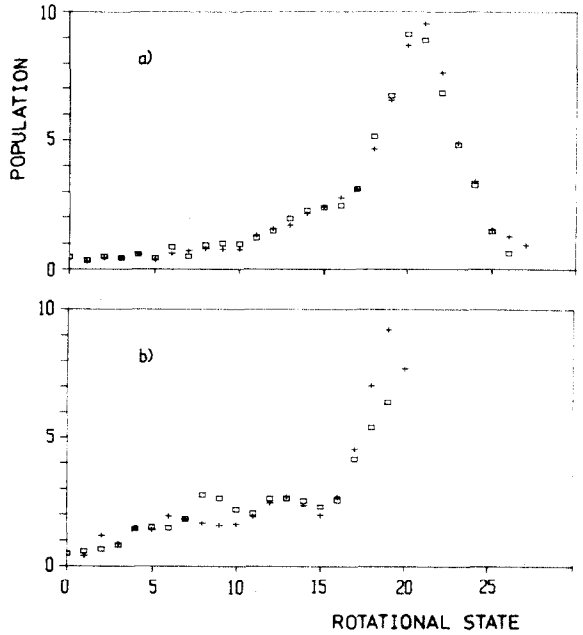

Fig. 3. Rotational state distributions for OH($A\,^2\Sigma^+$) in the vibrational ground state $v'=0$ (upper trace) and in the first excited vibrational state $v'=1$ (lower trace.) The two symbols refer to the two spin states F_1 and F_2.

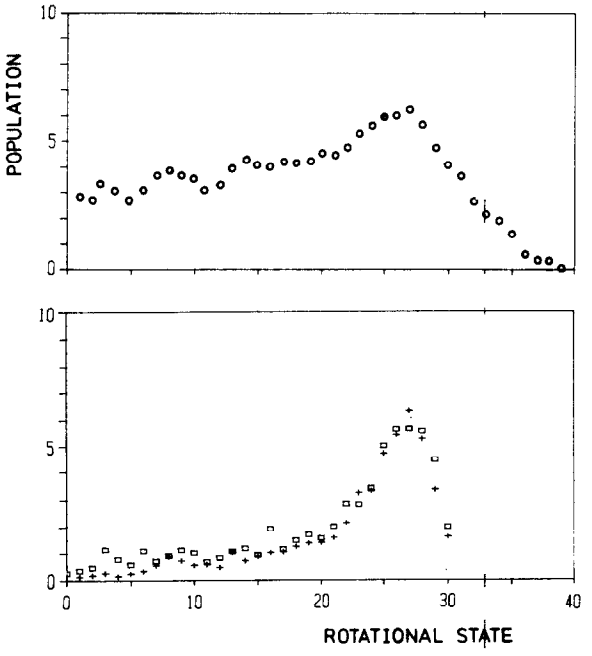

Fig. 4. Rotational state distributions for OD($A\,^2\Sigma^+$) in $v'=0$ (upper trace) and $v'=1$ (lower trace),

tion, fragment population in $v'=2$ is below the detection limit.

The rotational distribution as shown in fig. 4 is obtained by taking the sum of the population of both spin states, F_1 and F_2. This is only meaningful if the spin state population is statistical. For that reason the ratio

$$R_s = \frac{P(F_1)-P(F_2)}{P(F_1)+P(F_2)}$$

was determined and is represented in fig. 5. It can be seen from the figure that the assumption of the two spin states being populated statistically is valid for OH and for OD as well.

Table 1
Relative population of the vibrational levels of the OR($A\,^2\Sigma$) fragments formed in the photoexcitation of R_2O_2 at 157 nm

v'	OH($A\,^2\Sigma^+$)		OD($A\,^2\Sigma^+$)	
	$P(v')$(%)	$\bar{N}$	$P(v')$(%)	$\bar{N}$
0	92	21	91	27
1	8	20	9	27
2	<1	-	<1	-

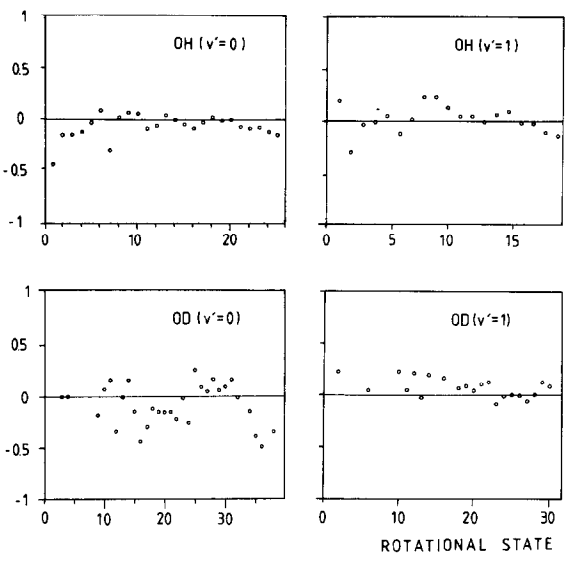

Fig. 5. Product state distribution of the spin components F_1 and F_2 in the $^2\Sigma^+$ state as a function of the rotational state N. A horizontal line at $R_s=0$ indicates that the dissociation process does not distinguish between the two spin–orbit states.

4. Fragment alignment

Many of the laser sources emit polarized light. This polarization may strongly influence the results if the observed line intensities will be directly converted into population numbers. For this reason isotropy of the photolysis and the fluorescence radiation was achieved before taking experimental data. But polarization of light on the other hand can provide valuable information on the fragmentation dynamics and if combined with Doppler spectroscopy is able to unravel the problem of finding the symmetry of the excited parent molecule state.

The use of linearly photolysis radiation aligns the absorbing parent molecules according to their transition dipole moment in such a way that maximum absorption is obtained if the $\boldsymbol{E}$ vector of the radiation field and the $\boldsymbol{\mu}$ vector of the transition dipole are parallel to each other. From symmetry reasons H_2O_2 exhibits only ^1A and ^1B electronic states with the electronic ground state being of ^1A geometry. For a $^1A \rightarrow {}^1A$ transition, $\boldsymbol{\mu}$ is parallel to the C_2 symmetry axis, whereas for a $^1A \rightarrow {}^1B$ transition $\boldsymbol{\mu}$ lies perpendicular to it. Excitation of a ^1A state will therefore lead to fragments with a preferred motion vertically

to the dipole moment. The result is a translational anisotropy expressed by a negative correlation between the transition dipole moment $\boldsymbol{\mu}$ and the fragment velocity $\boldsymbol{v}$.

In the case of a bent triatomic molecule, dissociating into an atom and a diatom the molecular fragment will rotate about an axis vertical to the plane of the triatomic parent. Since the transition dipole moment $\boldsymbol{\mu}$ has a fixed orientation to this plane, an angular correlation exists between the parent transition dipole moment $\boldsymbol{\mu}$ and the angular momentum $\boldsymbol{N}$ of the rotating fragment [19]. Due to the initial alignment of the parent there may be also an alignment of the fragment which is observable from the polarization characteristics of its emission if the fragment is simultaneously excited in the dissociation event. Observation of fragment alignment is therefore a source of information on the forces which drive the fragments apart.

Fig. 6 represents a view on the different orientations of the photolysis laser and the fluorescence detector. The collision frame x, y, z and the detector frame x', y', z' define the Euler angles ϕ, θ, χ. For linearly polarized incident light the emission intensity can be written according to ref. [7]:

$$I(\phi,\theta,\chi)=\tfrac{1}{3}I_0\{1-\tfrac{1}{2}h^{(2)}(J_iJ_f)A_0^{(2)}(J_i)\times[P_2(\cos\theta)-\tfrac{3}{2}\sin^2\theta\cos^2\chi]\},\qquad(2)$$

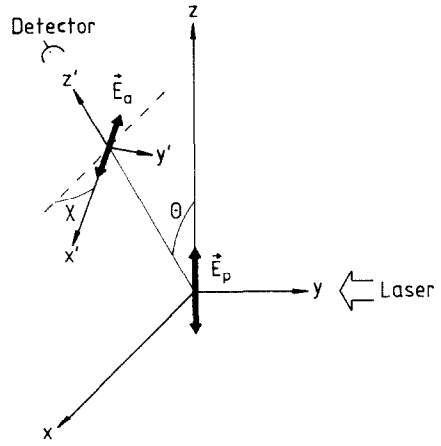

Fig. 6. Geometrical arrangement for the detection of aligned photofragments. The $\boldsymbol{E}_p$ vector of the linear polarized photolysis beam is parallel to the z axis. The emission is observed in the lab frame (x', y', z'), which is rotated by Euler's angles θ and χ versus the molecular frame (x, y, z).

in which $h^{(2)}(J_iJ_f)$ depends only on angular momentum quantum numbers of the initial (J_i) and final (J_f) fragment states. It takes the following values:

$$\begin{aligned}h^{(2)}(J_iJ_f)&=-J_i(2J_i+3)\quad\text{for P transitions,}\\&=+1\quad\text{for Q transitions,}\\&=-(J_i+1)/(2J_i-1)\quad\text{for R transitions.}\end{aligned}\qquad(3)$$

The azimuthal angle ϕ is irrelevant in problems having a cylindrically symmetric collision frame. Light intensities at two settings of χ are required. With $\theta=90°$ we obtain light intensities $I_\parallel$ and $I_\perp$ for two positions of the linear polarizer,

$$I_\parallel=I(\phi,\tfrac{1}{2}\pi,\chi=0),\qquad(4)$$

and

$$I_\perp=I(\phi,\tfrac{1}{2}\pi,\chi=\tfrac{1}{2}\pi).\qquad(5)$$

The polarization P and the polarization index R are then defined by

$$P=\frac{I_\parallel-I_\perp}{I_\parallel+I_\perp},\qquad(6)$$

$$R=\frac{I_\parallel-I_\perp}{I_\parallel+2I_\perp},\qquad(7)$$

which leads to the relation

$$P=\frac{3R}{2+R}.\qquad(8)$$

It follows for I_0 and $A_0^{(2)}$:

$$I_0=I_\parallel+2I_\perp,\qquad(9)$$

$$A_0^{(2)}=2R/h^{(2)}(J_iJ_f),\qquad(10)$$

so that the alignment can be easily determined from the measured polarization values.

The formulas describe light emission by fragments which are in a well defined quantum state $|i\rangle$. When the detected light is from two or more coherently excited closely spaced levels depolarization effects have to be considered. Hyperfine splitting causes such an

effect but often hyperfine precession is negligibly slow on the time scale of the radiative lifetime τ of the excited fragments. Yet there is still another depolarization effect possible due to an external magnetic field, H, which causes a precession of the fragment angular momentum about the magnetic field vector H. The frequency of this precession is given by

$$\omega = \mu_B g H/\hbar \tag{11}$$

with μ_B and g being the Bohr magneton and the Landé factor, respectively.

The observed polarization, P_{obs}, is reduced due to this effect. A correction is made by using the expression

$$P = P_{obs}[1 + (2\omega\tau)^2]. \tag{12}$$

Inserting the respective values for the earth magnetic field and the fragment lifetime we obtain values for P_{obs}/P above 0.9 for rotational quantum states $N \geqslant 10$.

In the actual experiment four settings were used in which the photolysis laser was linearly polarized either vertically or horizontally to the lab plane and the linear polarizer positioned vertical to the photolysis beam axis. Its settings were also either vertical or horizontal to the lab plane. Due to the cylindrical symmetry three of these four settings are identical ($I_\perp$), while the fourth setting leads to a different signal ($I_\parallel$).

The measured intensities $I_\parallel$ and $I_\perp$ were taken to extract the polarization index R according to eq. (7) and the fragment alignment $A_0^{(2)}(N)$, eq. (10), as a function of the rotational state N. The measured alignment of the OH($A\,^2\Sigma^+$, $v'=0$) fragment (fig. 7) is positive at very low rotational excitation and changes its sign for higher rotational states.

5. Discussion

Hydrogen peroxide with its screw configuration belongs to the point group C_2. The electronic ground state and the first excited electronic state are of ^1A symmetry while the second dissociative state is of ^1B symmetry [8–10]. At the wavelength of 157 nm a different electronic state of R_2O_2 is excited which correlates with a hydroxyl radical in the $^2\Sigma^+$ state. The excess energy E_{av} which is available to the fragments in this state is determined by the photon energy at 157.6 nm ($h\nu = 63450$ cm^{-1}), the internal energy $E_{int}(R_2O_2)$ of the parent molecule, the dissociation energy E_d, and the energy T_e which is needed to reach the lowest level of OR($^2\Sigma^+$) from the lowest level of OR($^2\Pi$):

$$E_{av} = h\nu + E_{int}(R_2O_2) - E_d - T_e. \tag{13}$$

The internal energy $E_{int}(R_2O_2)$ is mainly determined by the rotational energy of the parent $E_{rot}(R_2O_2) = \frac{3}{2}RT = 310$ cm^{-1}, and by the vibrational energy of the ν_4 torsional mode, $E_{vib}(H_2O_2) = 100$ cm^{-1} and $E_{vib}(D_2O_2) = 130$ cm^{-1}. At room temperature the other vibrational modes are only excited to a negligible amount. The energies which are used to calculate the energy partitioning in the various degrees of freedom are shown in table 2. The fraction of the available energy which is released as rotation and vibration in the OR($A\,^2\Sigma^+$) product is calculated in the usual manner:

$$f_r(A) = \sum_N P(N) E_{rot}(N)/E_{av}, \tag{14}$$

$$f_v(A) = \sum_v P(v) E_{vib}(v)/E_{av}, \tag{15}$$

where $P(N)$ and $P(v)$ are the product state distributions.

Only a minor part of the energy E_{av} is transferred into fragment vibration. The Franck–Condon principle can explain the low vibrational excitation. The equilibrium bond length of OR in the parent R_2O_2 ($r(R_2O_2) = 97$ pm) is comparable with the one in the free radical ($r(A\,^2\Sigma)_{OR} = 101$ pm). At photolysis wavelengths above 172 nm, only OR fragments in the electronic ground state are formed. The OR bond length of those radicals is $r(X\,^2\Pi)_{OR} = 97$ pm and the fragments exhibit essentially no vibrational excitation. This implies that the Franck–Condon factors for the decomposition of hydrogen peroxide to hydroxyl radicals in the $A\,^2\Sigma$ state should be mainly diagonal.

According to this model assumption excitation of water at 157 nm in its first absorption band should also yield vibrationless OH products. However, a significant amount of vibrationally excited fragments is found, because in this dissociation process an electron is raised from the nonbonding $1b_1$ to an antibonding $4a_1$ orbital resulting in an excitation of the symmetric stretch [20]. In contrast to the photofragmentation of water the photolysis of hydrogen peroxide should, therefore, involve a transition where the

Table 2
Energy partitioning (cm^{-1}) in the dissociation process $R_2O_2(\tilde{X}\,^1A)+h\nu(157.6\,nm)\rightarrow OR(X\,^2\Pi)+OR(A\,^2\Sigma^+)$

	E_d	E_{int}	E_{av}	$f_r(A)$	$f_v(A)$	$[f_t(A)]_{max}$
H_2O_2	197	4.9	178.8	44.3	1.7	27
D_2O_2	204	5.3	172.2	28	1.5	35

upper electronic surface shows only a small change in the dependence of the potential energy on the OR distance in R_2O_2.

The dominating feature in the photofragmentation of R_2O_2 at 157 nm is the extremely high rotational excitation of the OR($^2\Sigma^+$) product. More than 44% of the available energy are released in OH rotation and 28% in OD rotation. The rotational state distribution peaks at $N_{OH}=21$ ($E_{rot}(N_{OH}=21)\approx 8000$ cm^{-1}) and $N_{OD}=27$ ($E_{rot}(N_{OD}=27)\approx 7000\ cm^{-1}$) with a very narrow distribution of $\Delta N\approx 5$. An exception of this extremely narrow rotational distribution is the OD fragment in its vibrational ground state.

Before we will discuss the dissociation process in more detail, it is necessary to consider the conservation of linear and angular momentum which give further constraints on the product distribution. The conservation of total angular momentum, N_t, leads to the equation

$$N_t=N(R_2O_2)+N(h\nu)=N(X)+N(A)+L, \quad (16)$$

where $N(R_2O_2)$ is the initial parent rotation before excitation by a photon ($N(h\nu)=1\hbar$), $N(X)$ and $N(A)$ are the product angular moments in the electronic ground and excited state, and L is the orbital momentum of the recoiling RO–OR system. For thermal R_2O_2 the most probable parent rotation $\bar{N}(R_2O_2)$ can be calculated according to

$$\bar{N}(R_2O_2)=(IkT/\hbar^2)^{1/2}-\tfrac{1}{2} \quad (17)$$

if R_2O_2 is treated as rigid rotator with I being the moment of inertia. Rotation about the O–O internuclear axis gives a value of $\bar{N}(H_2O_2)\approx 3\hbar$, while rotation perpendicular to this axis leads to a value of $\bar{N}(H_2O_2)=10\hbar$. Thus, a total angular momentum of $N_t\approx 11\hbar$ has to be conserved. However, only rotation about the O–O bond can significantly influence product rotation, because any rotation perpendicular to this axis will mainly be transferred into fragment velocity and orbital momentum, due to the parent structure.

Let us now consider only a break of the O–O bond *without* any further influence of the upper potential surface on the fragment rotation. Initial parent rotation about the two axes of inertia perpendicular to the O–O axis will almost exclusively be transferred into fragment translation. A simple classical calculation shows that at most $1\hbar$ will be transferred into internal product rotation, while the overwhelming part of parent rotation is released as orbital angular momentum $l=\frac{1}{2}m_{OR}vs$, where s is the distance of the center of mass of R_2O_2 to the center of mass of the OR atoms in the parent, and v is the recoil velocity of the OR products after separation. Parent rotation about the O–O axis ($\bar{N}(H_2O_2)\approx 3\hbar$) will almost completely be transferred into product rotation. Therefore, the maximum total angular momentum of $N_t=1\hbar\,(h\nu)+3\hbar$ (parent rotation about the O–O axis) will be transferred into internal rotation of the OH(X)+OH(A) partner molecules and into orbital angular momentum (eq. (16)). The most probable rotation of electronically excited OH was found at $\bar{N}(OH)=21\hbar$. Therefore, at least $\bar{N}(OH)-N_t=21\hbar-4\hbar=17\hbar$ has to be supplied by the rotation of the simultaneously formed OH($X\,^2\Pi$) partner fragment and/or by the generated orbital momentum L. The corresponding conclusions in the photodissociation of D_2O_2 at 157 nm lead to a value of $\bar{N}(OD)-N_t=27\hbar-5\hbar=22\hbar$.

The orbital momentum L approaches its maximum value when all the remaining energy is transferred into translation, i.e. the OH($X\,^2\Pi$) partner product will have absolutely no internal excitation:

$$f_t(A)_{max}=f_t(X)_{max}=\tfrac{1}{2}[1-f_r(A)-f_v(A)]. \quad (18)$$

In a more state specific manner, a maximum of $E_t=\frac{1}{2}[E_{av}-E_r(\bar{N}(OH)=21)]$ can be transferred into translation of the OH($A\,^2\Sigma$, $\bar{N}=21$) fragment.

If we assume that the dissociation process can be

described by a simple repulsion along the O–O axis, then only a maximum momentum of $2\hbar$ can appear as orbital angular momentum L [12]. Obviously, this low value of L is not sufficient to fulfill the constraint of conservation of angular momentum.

Therefore, the OH(A) partner fragment, i.e. OH(X), has to be generated with high rotational excitation in order to conserve the total angular momentum. If the remaining energy for the OH(X) product is completely released as rotation, this rotational energy $E_{av}-E_r(\bar{N}(A))=81$ kJ/mol, corresponds to $\bar{N}(OH(X))\approx 19\hbar$ and the constraint

$$\bar{N}(OH(A))-\bar{N}(OH(X))\leqslant 4\hbar$$

is fulfilled. However, the rotational vectors $N(OH(A))$ and $N(OH(X))$ have to point in opposite directions.

Since a simple repulsive model can be excluded to describe the rotational excitation of the fragments, two different types of motion of the OR rotor during the dissociation process have to be considered: a bending like motion and a torsional motion of the OR in the parent R_2O_2.

If product rotation is induced only by a *torsional* motion, then the rotation of both OR partner fragments has to be exactly the same, but the rotational vectors, $N(OR(A))$ and $N(OR(X))$, point in opposite directions, as it is demanded to conserve the total angular momentum. In this case the translational and rotational motions of the products are strongly correlated with v_{OR} and N_{OR} being parallel to one another. This type of dissociation corresponds to a strong dependence of the upper potential energy on the dihedral (torsion) angle.

If product rotation is generated only by a *bending* motion of the OR rotor and we assume all other geometrical quantities to be the same as in the ground state configuration, then the angular momentum of the OR(X) is nearly perpendicular to that of OR(A) because of the dihedral equilibrium angle of $\chi\approx 120°$. Therefore, the OH rotation *cannot* compensate the observed $N(OH(A))$ and the total angular momentum would not be conserved. Thus, the decomposition of R_2O_2 can only proceed if a change of the dihedral angle χ is involved. Dissociation of planar peroxide in the trans position ($\chi=180°$) via a symmetric bending motion of the OR results in a parallel orientation of the OR(X) and OR(A) rotational vectors. Only a symmetric bending motion leads to the desired antiparallel orientation between $N(OR(X))$ and $N(OR(A))$. Vice versa, fragmentation of R_2O_2 with the R atoms at the cis position ($\chi=0°$) can only take place via an OR symmetric bending motion to conserve the total angular momentum.

The determination of the vector correlation between the transition dipole moment μ of the parent and the rotational vector N of the recoiling OR($A\,^2\Sigma^+$) fragment gives further information about the dynamics involved in the dissociation process. Any deviation of the alignment from zero implies an anisotropic distribution of $N(OR)$. At high OH(A) product rotations ($N>12$) the alignment is negative and approaches the value $A_0^{(2)}=-0.25$ (fig. 7).

A negative alignment corresponds to a more perpendicular orientation between μ and N. For a prompt dissociation process, e.g., the lifetime of the excited electronic state of parent peroxide is very short compared to its rotational period, the alignment is related to φ, the angle between μ and N:

$$A_0^{(2)}=\tfrac{4}{5}P_2(\cos\varphi). \qquad (19)$$

The measured alignment of $A_0^{(2)}=-0.25\pm0.025$ corresponds to a mean angle of $\varphi=69\pm2°$.

For simplification we assume a planar R_2O_2 configuration (C_{2h} symmetry) and an angle of φ at 90° because only the principle mechanism of the fragmentation process will be discussed. Fig. 8 shows the

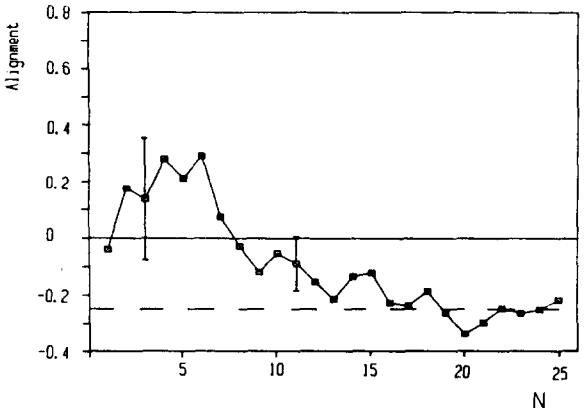

Fig. 7. Alignment $A_0^{(2)}(N)$ of OH($^2\Sigma^+$) product. The large negative value for high N indicates a more perpendicular orientation between N and μ, the transition dipole in the parent molecule.

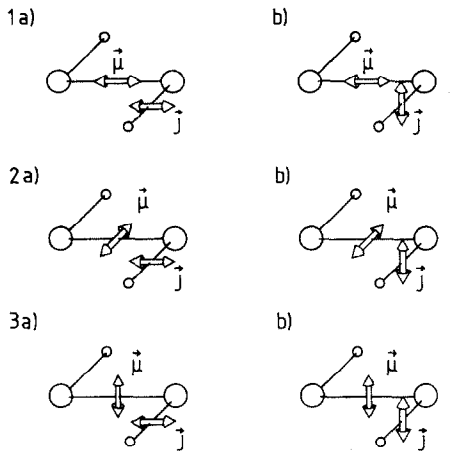

Fig. 8. Possible geometrical arrangments between the transition dipole moment in the parent and the rotational vector of the photofragment. (1a, b) $\mu \| O\text{–}O$; (2a, b) and (3a, b) $\mu \perp O\text{–}O$.

possible combinations of the alignment between μ and N. The transition dipole moment μ is either perpendicular to the C_{2h} symmetry axis (fig. 8, cases 1 and 2) corresponding to a $^1A \rightarrow {}^1B$ transition in the parent or parallel to C_{2h} (fig. 8, case 3) corresponding to a $^1A \rightarrow {}^1A$ transition. Since the fragments will rotate in the molecular plane of the parent (fig. 8b) or perpendicular to it (fig. 8a), six different combinations may occur. However, the observed angle φ between μ and N is close to 90° and, consequently, the two cases (1a, 3b) can be excluded in which μ and N are either parallel to the O–O axis or μ and N are perpendicular to the molecular plane. More detailed information about the fragmentation process can only be obtained if other vector correlations between μ, N, and v are known. These vector correlations can be extracted from measurements of the line shapes of the $OR(A\,^2\Sigma^+) \rightarrow OR(X\,^2\Pi)$ transitions. The spectral resolution in the present experiment was not sufficient to determine the profile of single lines. However, the consideration of the total angular momentum favors a torsional motion of the OR rotor during the dissociation process. Therefore, the cases (2a) or (3a) shown in fig. (8) should be favored to describe the dynamics of the fragmentation of hydrogen peroxide into two hydroxyl radicals, according to eq. (1).

The assumption of a product rotation generated via a torsional motion is also supported by ab initio calculations. The parent ground state shows only a minor energy dependence on the dihedral angle χ. However, all electronically excited states are extremely dependent (several eV) on the torsion angle χ and a high product rotation with N pointing essentially in the recoil direction will be induced.

The amount of rotation of both product molecules formed in the same dissociation process should be comparable. However, this generated rotation is further influenced by initial motion of the parent. Mainly parent rotation about the O–O axis will be transferred ($\approx 3\hbar$) into fragment rotation and should be superimposed on the OR rotation *induced* by the upper potential surface. This would cause a broadening of the rotational distribution. Since the observed product rotation is already centered tightly to the maximum value, the dominating part of the dissociation process must be extremely specific and all trajectories should end in very few product rotational states. Cooling of H_2O_2 in a supersonic jet will strongly reduce the initial parent rotation and a very narrow rotational state distribution should be observed ($\Delta N \ll 5$).

The observed alignment $A_0^{(2)} = -0.25$ for high product rotations is close to the lowest possible value of $A_0^{(2)} = -0.4$ which can only be reached if the transition dipole moment μ is perpendicular to the rotational vector N *and* if the dissociation is much faster than a rotation of the parent. We assume that the orientation between μ and the electric vector E of the photolysis laser, originally being parallel, will be disturbed by the rotational motion of the excited complex during the time of fragmentation. For a known orientation of the transition dipole, an upper limit of the lifetime of the excited H_2O_2 molecule can be calculated. A theoretical treatment of this behavior has been carried out by Nagata et al. [21] for a triatomic molecule ABC. We adopt this model for the H_2O_2 system, but regard one of the terminal hydrogen atoms as part of the neighboring oxygen atoms, (HO)–O–H. The "timer" in the dissociation process is given by the mean rotational period. For thermal H_2O_2 at room temperature we obtain a maximum lifetime of $\tau_m = 340$ fs if μ is perpendicular to the O–O axis and $\tau_m = 98$ fs if μ is parallel to the O–O bond. Certainly the real lifetime of the excited H_2O_2 complex will be much lower than the calculated value for $\mu \perp$ O–O, because any deviation of the assumed planar rectan-

gular molecule configuration will lower the extreme value ($A_0^{(2)} = -0.4$) for the alignment, even for an instantaneous fragmentation process.

The fragmentation of hydrogen peroxide at the excitation wavelength of 157 nm is well characterized by the measured scalar and vectorial properties of the OH(A) product. A decision concerning the geometry of the upper potential surface can be performed when the $\langle \mu, v \rangle$ correlation is known. High-resolution experiments are in progress in order to resolve the profile of single emission lines and to determine all relevant vector correlations in the photodissociation process.

Acknowledgement

The work has been performed as part of a special programm of the Deutsche Forsachungsgemeinschaft (DFG). Financial support is gratefully acknowledged.

References

[1] Th. Winkler, Diplom Arbeit Ffm. (1987).
[2] H. Schiff, G.W. Harris and G.I. McGray, in: Monitoring of gaseous pollutants by tunable diode lasers, eds. R. Grisar, H. Preiser, G. Schmidtke and G. Restelli (Reidel, Dordrecht) pp. 4–47.
[3] M. Suto and L.C. Lee, Chem. Phys. Letters 98 (1983) 153.
[4] G.H. Dieke and H.M. Crosswhite, J. Quant. Spectry. Radiative Transfer 2 (1962) 97.
[5] R.N. Zare and D.R. Herschbach, Proc. IEEE 51 (1963) 173; G.E. Bush and K.R. Wilson, J. Chem. Phys. 56 (1972) 3638, 3655; C. Jonah, J. Chem. Phys. 55 (1971) 1915; J. Solomon, C. Jonah, P. Chandra and R. Bersohn, J. Chem. Phys. 55 (1971) 1908.
[6] S. Klee, K.-H. Gericke and F.J. Comes, J. Chem. Phys. 85 (1986) 40.
[7] R.N. Dixon, J. Chem. Phys. 85 (1986) 1866.
[8] K.-H. Gericke, S. Klee, F.J. Comes and R.N. Dixon, J. Chem. Phys. 85 (1986) 4463; K.-H. Gericke, S. Klee and F.J. Comes, Chem. Phys. Letters 137 (1987) 510.
[9] M.P. Docker, A. Hodgson and J.P. Simons, Faraday Discussions Chem. Soc. 82 (1987) 25.
[10] A.U. Grunewald, K.-H. Gericke and F.J. Comes, Chem. Phys. Letters 132 (1986) 121; J. Chem. Phys. 87 (1987) 5709; J. Chem. Phys. 89 (1988) 345.
[11] K.H. Becker, W. Groth and D. Kley, Z. Naturforsch. 20a (1965) 748.
[12] H. Gölzenleuchter, K.-H. Gericke, F.J. Comes and P.F. Linde, Chem. Phys. 89 (1984) 93.
[13] P.A. Giguère and P. Geoffrion, Can. J. Res. B 27 (1949) 168.
[14] J.P. Simons, A.J. Smith and R.N. Dixon, J. Chem. Soc. Faraday Trans. 80 (1984) 1489.
[15] J. Brzozowski, P. Erman and M. Lyra, Physica Scripta 17 (1978) 507; K.R. German, J. Chem. Phys. 62 (1975) 2584; P.M. Selzer and G.C. Wang, J. Chem. Phys. 71 (1979) 3786.
[16] J.A. Coxon, J. Mol. Spectry. 58 (1975) 1.
[17] W.L. Dimpfl and J.K. Kinsey, J. Quant. Spectry. Radiative Transfer 21 (1979) 233.
[18] K.R. German, J. Chem. Phys. 62 (1975) 2584; 63 (1975) 5252; R.A. Sutherland and R.A. Anderson, J. Chem. Phys. 58 (1973) 1226.
[19] C.H. Greene and R.N. Zare, Ann. Rev. Phys. Chem. 33 (1982) 119.
[20] P. Andresen, G.S. Ondrey, B. Titze and E.W. Rothe, J. Chem. Phys. 80 (1984) 2548.
[21] T. Nagata, T. Kondow, K. Kuchitsu, G.W. Loge and R.N. Zare, Mol. Phys. 50 (1983) 49.